Morphotectonics of the Concud Fault (Iberian Chain, Spain): Comparing Geomorphic and Geologic Indices of Activity of an Intraplate Extensional Fault

Paloma Lafuente[1], Teresa Lamelas[2], José L. Simón[1*], Mª Asunción Soriano[1]

1 *Dep. Ciencias de la Tierra, Universidad de Zaragoza, E-50009 Zaragoza, Spain*.

2 *Dep. Geografía y Ordenación del Territorio, Universidad de Zaragoza, E-50009 Zaragoza, Spain.*

* Corresponding author.

E-mail address: jsimon@unizar.es

Tel: 34 976 76 10 95 – *Fax*: 34 976 76 11 06.

Short title: Morphotectonics of the Concud Fault

Morphotectonics of the Concud Fault (Iberian Chain, Spain): Comparing Geomorphic and Geologic Indices of Activity of an Intraplate Extensional Fault

Abstract

The results of geomorphic analysis of the Concud fault-generated mountain front (central Iberian Chain, Spain) are introduced into classifications of fault activity proposed by previous authors, and compared with slip rates calculated from geologic markers. The Concud fault is an extensional structure active since the mid Pliocene times. It gives rise to a 60 to 120 m high mountain front, where footwall rocks belonging to the Triassic and Jurassic (north-western sector) and Miocene (south-eastern sector) crop out. Conspicuous triangular facets are preserved on Jurassic rocks of the central sector, while short, generally non-incised alluvial fans make the piedmont. The value of the Mountain-front sinuosity index is $S_{mf} = 1.24$ for the whole mountain front (1.17 and 1.32, respectively, for both segments showing distinct footwall lithology), as obtained by the most conservative procedure. Average valley floor width/height ratios calculated for seventeen gullies crossing the fault are $V_f = 0.30$ (250 m upstream from the fault trace) and $V_f = 0.22$ (500 m upstream). These geomorphic indices, together with qualitative features of the escarpment and piedmont landscape, indicate 'moderate' to 'rapid' fault activity. The range of slip rates estimated from such morphotectonic classification (0.03 to 0.5 mm/y) encloses the range calculated from offset Late Pliocene and Pleistocene stratigraphic markers (0.07 to 0.33 mm/y). Nevertheless, the highest potential slip rate (0.5 mm/y) clearly represents an overestimate: the mountain front could give the impression of an anomalously high level of activity owing to episodic rejuvenation caused by base level drop.

Key words: active fault, slip rate, morphotectonics, geomorphic index, Jiloca graben.

1. Introduction

The level of activity in recent faults can be assessed by observing and analysing their geomorphologic expression. This line of research is particularly useful in the case of intraplate faults, in which rates of activity are generally orders of magnitude lower than those in interplate regions, and geologic evidences are often scarce or difficult to obtain. The geomorphological criteria can be applied to broadly identify active structures, as well as to make a quantitative approach of their velocity of displacement, based on the general notion that the rates and patterns of surficial processes that produce and modify landforms match the rates and patterns of deformation [1, 2].

Mountain fronts produced by dip-slip faults constitute the most prominent landforms revealing tectonic activity in continental regions. Besides, the drainage networks transverse to them are also sensitive to tectonic movements, mainly short gullies, which are not as capable as large rivers to recover their longitudinal and transversal profiles after vertical earth movements [3]. Morphotectonic analysis of faulted areas is usually carried out by applying specific geomorphic indices [4, 5], which allow objective comparison and assessment of landscape features. Values obtained for them, together with other qualitative features of the associated landforms, serve as an input for classifications of fault activity, such as those proposed for semiarid regions by Bull and McFadden [5], Bull [6], McCalpin [7] or Silva *et al*. [8]. Regional studies of tectonic mountain fronts have shown how slip rates estimated from those classifications fairly approach those obtained from independent, geologic evidence (e.g. [9]).

On the other hand, fault activity can also be directly quantified by calculating slip rates from geological data, i.e. by measuring offsets in well-defined and dated stratigraphic markers. Obviously, faults in which both approaches, geological and morphometric, can be independently achieved allow us to check the validity of the aforementioned classifications.

In the present paper, we compare the results of this double methodology for an extensional fault located in the central Iberian Chain (eastern Spain): the Concud fault. This is an active fault whose structural, stratigraphical and chronological setting is well known at present. Slip rates have been calculated both for its overall period of recent activity (taking into account geological information on map scale), as well as for short time spans in which coseismic displacements have been evidenced from trench study [10, 11, 12, 13, 14]. At the same time, its geomorphological expression is enough clear and comprehensible for allowing a precise morphometric analysis using detailed topographic maps and a Digital Elevation Model.

Our objectives are: (1) to estimate the level of activity of the Concud fault by means of both independent methodologies (slip rates from offset stratigraphic markers, and morphotectonic analysis), comparing and discussing their results within the framework of extensional structures of the eastern Iberian Peninsula; (2) to check the adequacy of classifications of fault activity based on geomorphic criteria under tectonic and climatic conditions such as those currently found in the interior of the Iberian plate.

2. Geological and geomorphological setting

The Iberian Chain is an intraplate chain that shows moderate instrumental and historic seismicity, but contains a number of conspicuous active faults at its central and eastern sectors. These faults belong to a Neogene-Quaternary graben system that postdate the compressive structures and are genetically related to the rift at the Valencia Trough [15, 16, 17]. The grabens evolved through two distinct extensional episodes [15, 16]: the first one (Miocene) produced NNE-SSW trending structures, particularly the Teruel graben (Fig. 1); the second one (Late Pliocene-Quaternary) gave rise to the NNW-SSE trending Jiloca graben and reactivated the former ones.

The Teruel basin is a half graben with an active eastern boundary made of large N-S striking faults (Fig. 1). These faults produce prominent mountain fronts that separate the graben bottom (usually at 800-1000 m.a.s.l.) from the El Pobo and Javalambre massifs (at about 1700 and 2000 m, respectively). The basin is filled with Neogene sedimentary units made of red clastic alluvial deposits, and lacustrine carbonates and gypsum. Their ages, well constrained by numerous mammal fossil assemblages [18, 19], range from the Vallesian to the Ruscinian (Late Miocene-Early Pliocene).

The Jiloca basin constitutes a large intramontane topographical depression with a smooth bottom at about 1000 m.a.s.l. bounded by ranges and plateaus at 1200 to 1500 m. Its overall NNW-SSE trend results from an en-échelon, right releasing arrangement of NW-SE-striking normal faults, the largest ones being located at the eastern boundary: Calamocha, Sierra Palomera and Concud faults (Fig. 1). This trend is essentially controlled by the dominant ENE-WSW extension direction characterizing the recent stress field [20, 21]. The visible infill of the Jiloca graben is constituted by an Upper Pliocene to Pleistocene sedimentary sequence made up by alluvial fan, pediment and episodic palustrine deposits, which is underlain at the central sector by marls of probable Neogene age (only observed in boreholes [22]).

The Concud fault is a 14.2 km-long structure that bounds the southernmost sector of the Jiloca graben (Figs. 1, 2). It shows an overall WNW-ESE strike, which veers towards N-S near its southern termination. Dips measured at the outcropping fault surfaces typically range from 65 to 70º SW. The observed striations indicate a nearly pure normal movement. The fault usually makes the contact of Pleistocene alluvial deposits of the hanging wall with Triassic and Jurassic units of the footwall at the western and central sectors, and with the Neogene units of the Teruel basin at the southeastern one. At the central sector, a double fault trace has been recognized; the southern trace separates the Plio-Quaternary alluvial deposits from Lower Triassic (red clastic Buntsandstein facies), while the northern one separates Lower Triassic from Lower Jurassic units.

The fault trace follows the nearly vertical limb of a NW-SE trending anticline (Fig. 2), which suggests that the extensional structure represents the negative inversion of a previous reverse fault associated to the fold [12, 14]. The extensional movement, as far as has been geologically documented, begun by the latest Ruscinian (mid Pliocene), cutting the previous Upper Miocene-Lower Pliocene infill of the Teruel basin (Fig. 2). Sedimentation was then interrupted on its footwall, whereas a complete syntectonic, Villafranchian sequence was deposited on the hanging wall [16, 23]. The Villafranchian sediments include palustrine carbonates, red clastic alluvium and a pediment cover. The Pleistocene sediments essentially belong to alluvial fans spreading from the mountain front; they have yielded OSL (Optically Stimulated Luminiscence) ages ranging from 77 ± 4 ka to 20 ± 1 ka [12, 14, 24].

Apart from the conspicuous imprint of tectonics, the landscape of the junction area between the Teruel and Jiloca grabens has undergone intense fluvial modelling during the Quaternary by the Alfambra-Guadalaviar river system. Three main Pleistocene terrace levels have been described in this area [18, 25], some of them locally splitting into two sublevels [26, 27]. The Upper Terrace (85-90 m above talwegs) is of unknown age. The Middle Terraces (45-65 m, with a local sublevel at 40-45 m) have yielded diverse absolute U/Th, TL and OSL ages ranging from 250 ± 32 ka to 90 ± 5 ka [14, 24, 28, 29]. The Lower Terraces (20-30 m, with a local sublevel at 15-20 m) have also OSL absolute dating, with ages ranging from 22.0 ± 1.6 ka to 15.0 ± 1.0 ka [14, 24]. The youngest, Holocene terrace level (3-5 m) represents the flood plain of the main rivers; at the Alfambra valley, it has provided an OSL age of 3.4 ± 0.7 ka [14, 24].

3. Slip rates from the geological record

The Concud fault has been active during most of the Late Pliocene and Quaternary times. Slip rates have been calculated both for the whole fault activity period and for distinct time lapses within the Middle-Late Pleistocene, which allows us to estimate certain variability in slip rate through time (Table 1).

Calculation of the average slip rate for the overall extensional history is based on the position and age of the uppermost pretectonic level, i.e. the top of the mid Pliocene lacustrine deposits at the footwall (Figs. 2, 3a). These make a structural platform at 1180-1200 m.a.s.l. (Celadas plateau), and are dated by paleontological methods in 3.6 Ma (latest Ruscinian, MN 15b biozone [18, 19, 30]). At the hanging-wall, the same stratigraphic level appears at 920-940 m.a.s.l., lying unconformably beneath the Upper Pliocene and Pleistocene red clastic sediments of the Jiloca graben (e.g. at Concud village). This indicates a minimum post-Early Pliocene vertical offset of about 240 m. Considering an average dip of 70º and a pure normal movement, this results in a minimum net displacement of 255 m and a slip rate of 0.07 mm/y [10, 12]. This calculation has been refined by Lafuente [14] after reinterpreting the structure of accommodation folds within the hanging wall, resulting in a net displacement within the range of 240-360 m and a slip rate of 0.07-0.10 mm/y (most probable values of 290-300 m and 0.08

mm/y).

Slip rates since Middle Pleistocene times have been inferred at Los Baños (see location in Fig. 2). At this site, the Middle Terrace of the Alfambra river, with a tufa level at top dated between 169±10 and 116±4 ka, shows a minimum throw of 36h m, then a net displacement of 39 m [10, 12], which provides a slip rate of 0.23 to 0.33 mm/y (Fig. 3b). If we consider other different ages published by Gutiérrez *et al*. [24] for the aforementioned tufa (250+32/-25 and 213+33/-26 ka, not as reliable as the former ones, according to Lafuente *et al*. [13], the resulting slip rate would range from 0.16 to 0.33 mm/y, still significantly higher than the overall rate from mid Pliocene times. Besides, a recent trench study carried out at this site [12, 13, 14] has allowed an independent estimate for the Late Pleistocene slip rate. Five (perhaps six) large single paleoseismic events, chronologically constrained between 71.7±5.2 and 32.1±2.0 ka, globally represent an accumulated displacement of 10-12.5 m, therefore providing a rate of 0.25-0.31 mm/y.

Data on Late Pleistocene slip rates are also available from the central sector of the fault (El Hocino site), where two paleoseismological trenches have been recently studied [11, 14]. The youngest pediment surface is apparently offset giving rise to a gentle, 5.0 to 6.3 m high topographic escarpment, then confirmed by trenching as a branch of the Concud fault (Fig. 3c). The alluvial cover of the pediment has been dated by OSL (48.9±4.4 ka), although the artificial reworking (cultivation) of the uppermost deposits makes the result not completely reliable. A vertical slip rate of 0.10-0.13 would be obtained, as a first approach, considering those data. More precise results have been obtained from one of the surveyed trenches, where the lithologic unit representing the pediment cover in the hanging wall of the exposed fault was recognized and dated. It lies in geometric continuity with the pediment surface at this block, and it is deformed into a roll-over geometry underlying a syntectonic, wedge-shaped sedimentary sequence (Fig. 3c). A fault throw of 5.5 m has been inferred in cross-section for this morpho-sedimentary marker; considering the dip of the shallow fault surface (70º SW) and the pitch of the dominant fault striation (75º S), a net slip of 6.1 m can be approached. The age of the marker is bracketed between 77.3±4.3 and 74.2 ±8.2 ka OSL, probably closer to the latter [11, 14]. The resulting net slip rate is 0.08 mm/y.

4. Morphotectonic analysis

4.1. Mountain front, fluvial network and piedmont landscape

The Concud fault is expressed in the landscape by a fault-generated mountain front 60 to 120 m high and 12.3 km long (Fig. 4a). A portion of the total fault length (1.9 km), close to the SE tip, does not show any clear morphologic escarpment. The mountain front is dissected by transverse stream channels, which model some well-preserved triangular facets at the central sector where the free face of the main escarpment is made of Jurassic limestones (Figs. 4b, 5a). These facets have absolute height differences between the toe and the peak ranging from 60 to 100 m, and quite steady mean slopes of 22.5º to 23º, which involves a significant decline with respect to the original slope of the fault scarp. A detailed topographic profile of one of these facets (Fig. 5b) shows a convex-straight-concave shape with a maximum midslope angle of 25º. Such profile would corresponds to a long-lived, essentially wash-controlled slope, which has graded into a relatively steady form according to a dominant decline mechanism [31, 32]. The latter has been probably favoured by the fact that the drainage divide is relatively far from the top of the escarpment [32]. Slope retreat has an almost negligible contribution to the final landscape. It is significant only where relatively soft Upper Triassic sandstones crop out at the footwall. The maximum horizontal distance measured between the fault trace and the toe of the escarpment in such cases is about 20 m.

Diverse categories of transverse stream channels can be distinguished along the mountain front (Fig. 4a):

(I) Major, plurikilometre-scale gullies, whose drainage basins largely enter the Neogene rocks of the Celadas plateau exhibiting a dendritic pattern (basins designed as 7, 8, 9, 15 and 17 in Fig. 4a). They are connected to the regional fluvial network through the main collector Barranco de Concud (except gully 17).

(II) Middle, kilometre-scale gullies whose drainage basins partially enter the upthrown block. Most of them drain the folded Jurassic rocks at the western sector (numbers 12, 13, 14 and 16); others show limited entrance into the Neogene platforms at the eastern one (numbers 6 and 6’). Generally, they are not connected to the external fluvial network, except in the case of gully 14, which is tributary of 15. Channel 12 (Bco. de la Hoz in Fig. 4b) represents a particular case: it is interrupted at the head of the pediment, at a fault-relay zone of confuse drain setting, while a distinct gully (although bearing the same toponym) initiates close to it and finally joints the main external collector.

(III) Shorter, hectometre-scale gullies whose heads are located close to the top of the mountain front (numbers 1, 2, 3, 4, 5, 5', 8', 10, 10', 11, 12', 12" and 13'). Only channels 10 and 11 continue into the external fluvial network; the rest suddenly disappear when attaining the downthrown block, or grade into shallow courses that vanish at a short distance within the pediment.

(IV) Minor, hectometre-scale gullies constrained within the triangular facets or within the strict fault escarpment (not numbered in Fig. 4a). All them systematically disappear as they abut the pediment head.

Such diversity of fluvial courses also involves diversity in size and shape of the drainage basins, which reflects distinct development stages of the fluvial network as a response to both the inherited structural grain and the active fault. Most basins developed on the Neogene units (eastern sector) exhibit the symmetric, 'wine-glass' shape that characterizes fault-generated fluvial networks [32], either circular (3, 6, 8') or elongated (2, 5, 7, 8, 9). Their length systematically decreases eastwards, as they approach the Alfambra valley, suggesting that the erosive potential of the latter on the Neogene soft materials has inhibited the small transverse drainage basins to grow. Among the basins developed on Jurassic rocks of the western sector, only a number of category III, circular basins delimiting triangular facets (12', 12", 13) exhibit regular size and shape. Basins of categories I and II are heterogeneous in size (depending on whether their heads enter or not the Neogene units of the Celadas plateau) and strongly asymmetric (controlled by the inherited, WNW-ESE structural direction).

Spacing of drainage outlets shows certain regularity, in spite of the diverse scales and shapes of drainage basins. At the western sector, on a lithologically and structurally homogeneous substratum, channels of categories III and IV are regularly spaced. At the eastern sector, a progressive westwards increase of spacing can be observed, which parallels the progressive increase of channel length and area of drainage basins (1 to 9 in Fig. 4a).

We have briefly analysed the ratio of the length of drainage basins (mean distance between the fault trace and the drainage divide, measured in a direction perpendicular to the mountain front) to the mean spacing of the outlets along the fault trace [33, 34, 35, 36]. This ratio has been calculated separately for gullies of each category I to IV. Mean spacing has been computed from distances between outlets corresponding to neighbour drainage basins belonging to the same category, according to the procedure proposed by Walcott and Summerfield [36]. The results are shown in Table 2, which shows values of length-to-spacing ratios ranging from 1.22 to 2.47. In our opinion, comparison with values published by other authors should be made only for gullies of category III (basins that drain from the ridge crest of the fault block; Type i of Talling *et al*. [35]; Type 1 of Walcott and Summerfield [36]). Therefore, a ratio of 1.97 should be considered in our case.

This value closely approaches 2.0, the spacing ratio that many authors have typically reported from tectonic mountain fronts developed in distinct tectonic settings and at different scales. In particular, it is close to values calculated by Hovius [34], for a number of thrust-generated range fronts all over the world except for the Himalayas (1.91-2.23), and Walcott and Summerfield [36], for the southeast African passive margin (1.89). Our ratio also lies within the range obtained by Talling *et al*. [35] along active extensional fault blocks in SW United States (1.41-4.06, mean: 2.5), although the authors acknowledge that in this case both the mean and the variability are greater than those observed in linear mountain belts.

A high number of short alluvial fans (from 0.1 to 2 km in length) develop from the mountain front (Fig. 4b). They show moderate to high slope (up to 7-8º at their apexes) that, in any case, clearly contrasts with the midslope angle of facets (Fig. 5b). In general, larger, older alluvial fans are related to gullies of categories I and II, and are subsequently incised by them. In contrast, short gullies of categories III and IV, deeply incised into the footwall and suddenly vanishing as they enter the Quaternary deposits of the hanging-wall, produce smaller alluvial fans (typically, 300-500 m long for those of category III, and 100-150 m long for those of category IV) (Fig. 4b). This broadly indicates that the rate of subsidence of the hanging-wall block has been lower than the rate of downcutting of the large streams, but higher than that of minor gullies. The apexes of the alluvial fans do not onlap the upthrown fault block, but are cut at the fault trace, which constitutes a further evidence of active tectonics [6].

4.2. Geomorphic indices: methodological remarks

The morphotectonic analysis carried out for estimating the degree of activity of the Concud fault has been based on three classic geomorphic indices:

(a) Stream-gradient index (*SL*), developed by Hack [4]. It is defined for a given stream reach: $SL = L\ \Delta H/\Delta L$, where $\Delta H/\Delta L$ is the channel gradient of the reach, and L is the distance from the drainage divide measured along the channel. The *SL* index crudely reflects the available stream power. Anomalously high *SL* values are related to either highly resistant rocks or maladjustment of the channel profile to recent tectonic activity or climatic changes [2, 37]. Once rejected lithologic and climatic factors, such high *SL* values are a valuable tool in detecting and assessing active tectonic structures involving vertical displacement. *SL* values along distinct channels can be normalized by comparing each one with the *gradient index K* of the entire profile: $K = \Delta H_T / \ln L_T$, where H_T is the total height difference between head and outfall, and L_T is the total length. The ratio *SL/K* is then used for identifying profile anomalies of regional significance (e.g. Seeber and Gornitz [38]).

(b) Valley width/height ratio (V_f), proposed by Bull and McFadden [5]. It is defined for a given valley section: $V_f = 2V_{fw} / [(E_{ld}–E_{sc}) + (E_{rd} –E_{sc})]$, where V_{fw} and E_{sc} are the width and the elevation of the valley floor, and E_{ld} and E_{rd} are the elevations of the left and right valley divides, respectively. Measured at a specified distance from a fault trace, it reflects the effectiveness of fluvial incision in response to active tectonic elevation (low V_f values) versus lateral erosion due to stability of the base level (high V_f values) [37].

(c) Mountain-front sinuosity index (S_{mf}), proposed by Bull and McFadden [5]. It is measured for a given segment of a tectonic mountain front: $S_{mf} = L_{mf} / L_s$, where L_{mf} is the complete length along the mountain-piedmont junction, and L_s is the overall length of the mountain front. This index reveals the balance between incision of gullies into the upthrown block, which tends to increase sinuosity, and fault activity, which tends to maintain a nearly straight escarpment. A sinuosity close to 1 can be interpreted as a result of active faulting, whereas values close to or over 2 indicate an embayed, low activity range front [2].

Measurements needed for obtaining indices *SL* and V_f have been acquired from a Digital Elevation Model (DEM) (Fig. 5a). This has been developed using a topographic map at a 1:5,000 scale, available at SITAR (Servicio de Información Territorial de Aragón; Aragón regional Government, Spain). Sixteen CAD files were downloaded from the SITAR website [39], imported into ArcGIS 9.2. (ESRI Inc., Redlands, California). The contour lines and elevation points where revised, in order to find anomalous values, and used as mass point to develop a triangulated irregular network (TIN) with the '*Create Tin from feature'* functionality on the *3D Analyst* toolbar. Then a raster surface, pixel size 5x5 m, was developed using the *'Tin to Raster'* geoprocessing tool.

Seventeen gullies long enough to provide representative results were selected for calculating *SL* indices (see location on Fig. 4a). Measures were taken at regular height intervals (each 5 m) on their talwegs.

The V_f ratio has been calculated on the same gullies, 250 and 500 m upstream from the fault trace, as specified by Silva *et al*. [8] and McCalpin [7], respectively, for their classifications of fault activity. Since the DEM used for morphometric calculations has a 5 m-wide pixel, we have taken this value as a minimum for every measured valley width (V_{fw}). This prevents from risk of underestimating such width, which would produce artificial exaggeration of the Vf ratio.

For calculating the S_{mf} index, we should take into account that the length of the sinuous mountain front (L_{mf}) is a fractal parameter whose exact value depends on the scale of the map where the measurements are taken. Bull and McFadden [5] and Silva *et al*. [8] proposed to use topographic maps at scales from 1:62,500 to 1:250,000, and 1:50,000, respectively. However, owing to the moderate length of the Concud fault, we have preferred to measure L_{mf} on a 1:12,500 orthoimage, bearing in mind that this could involve an overestimate of the sinuosity, therefore an underestimate of the degree of fault activity. The lengths have been computed by means of a digital curvimeter, averaging a set of 5 measures for each analysed quantity.

Another element of uncertainty when the S_{mf} ratio is calculated comes from the notion of *overall length* of the mountain front enunciated by Bull and McFadden [5]. This parameter has been historically considered as either the *straight length* [1, 8, 37] or the length of the broadly curved envelope of the mountain front (e.g. Yeats *et al*. [40]; also implicit in maps by Bull and McFadden [5]). The first option seems not to be adequate in cases of fault escarpments exhibiting strongly curved traces. The bias induced by trend variation, as well as by sharp changes in lithology or drainage setting, can also be prevented by separating the total length of the mountain front into distinct segments according to such heterogeneities [41]. We have adopted these criteria, comparing S_{mf} values obtained from different procedures, both for two lithologically differentiated segments and for the whole mountain front.

Introducing these geomorphic indices into the classifications proposed by McCalpin [7] (adapted from Bull and McFadden [5]) and Silva *et al*. [8] allows us to assess the level of fault activity. Further geomorphological evidences concerning the presence of triangular facets, relationships between alluvial fans and river incision, and shape of valley sections are also used as an input for such classifications.

4.3. Geomorphic indices: *results and interpretation*

The discrete *SL* values calculated from the longitudinal profile of each surveyed gully (Fig. 6a) have been integrated into a distance–*SL* curve (Fig. 6b). Each curve displays one or several relative maxima that conspicuously stand out above the 'basal tendency' (straight line superposed on each curve of Fig. 6b, which reveals a slow and continuous downstream increase of *SL* values). Such sharp peaks have local *SL* values several times higher than the *gradient index K* for the entire profile. An arbitrary value $SL/K = 5$ has been marked on SL curves as a threshold for filtering significant profile anomalies (segments identified by thick traces on profiles of Fig. 6a, following Seeber and Gornitz [38]).

Among such anomalies, several (open dots) are clearly related to lithology (usually, presence of hard Jurassic limestones or dolostones). Others (solid triangles) can not be explained by lithology and almost systematically appear at a short distance upstream from the fault trace (vertical, dotted line in Fig. 6). This strongly suggests that the tectonic vertical displacement is responsible for the sharp increase of stream gradient, generating topographic knick points that migrate upstream from the fault.

Only a few exceptions split away from this general tendency, most of them associated to gullies within the zone where a double fault trace was mapped. First, no *SL* peak appears at gully 6 close to any of the two fault traces; two maxima located upstream are related to hard Jurassic rocks. Gullies 7, 9 and 10 show knick points (*SL* peaks) associated to the northern fault trace, but not to the southern one; this indicates a lower slip/downcut rate on the footwall of the southern fault. In contrast, a second maximum appears downstream within the downthrown block in gullies 5 and 13, which suggests that the southern fault could have propagated beneath both of them in spite of the lack of surficial geologic evidence.

In general, tectonic uplift seems to have perturbed the gradients of small streams (short gullies with a smaller catchment area; in particular, gullies 2 to 5) more strongly than those of the major ones (gullies 7 to 15 and 17). This pattern fits the observation by Merrits and Vincent [3] relative to the different response of 1st, 2nd and 3rd order streams to tectonic uplift. Larger streams are able to maintain their longitudinal profiles more efficiently, whereas smaller streams may not downcut at the same rate as the local base level is tectonically lowered [2].

The analysed gullies show cross sections characterized by a soft V-shape. V_f values measured 250 m upstream from the fault trace range from 0.11 to 0.88 (mean: 0.30); those measured 500 m upstream range from 0.06 to 0.40 (mean: 0.22) (Fig. 7). As a rule, in our study area, this index mainly depends on lithology. Lower values (narrower valleys) are found in the hard Jurassic rocks of the northwestern sector (gullies 9 to 16), whereas higher values correspond to relatively soft Neogene rocks of the southeastern one (gullies 1 to 8).

The same lithologic domains have been distinguished for calculating the S_{mf} index, also taking into account that the dominant morphologic escarpment switches from the northern to the southern fault trace as the lithologic change occurs (Fig. 8). The NW segment (A-B), where Jurassic carbonates make the mountain front, has yielded S_{mf} = 1.17 (Table 3). For the SE segment (C-D), dominated by Miocene clastic and carbonate deposits, S_{mf} = 1.32. The lower sinuosity at the NW segment is consistent with the lower erodibility of the Jurassic limestones and dolostones. We discard that such contrast in S_{mf} values could represent a significant difference in slip rates for both segments during recent times, i.e. a hypothetical evidence of seismic segmentation of the fault. Calculating the sinuosity index for the whole mountain front, we obtain an intermediate value S_{mf} = 1.24. We should explain that these quantities result from the conservative calculation that uses the straight length of the mountain front as divisor ($L_s = L_{ss}$), as required for applying the classification by Silva *et al*. [8]. If the length of a broadly curved envelope is considered ($L_s = L_{sc}$), the resulting S_{mf} values are 1.08 and 1.26 for both separate segments, and 1.18 for the whole mountain front, respectively. In any case, the values are significantly low, so indicating a noteworthy level of fault activity.

4.4. Using geomorphic attributes for classifying fault activity

The calculated V_f and S_{mf} geomorphic indices have been entered into the classifications proposed by McCalpin [7] and Silva *et al*. [8] in order to characterize the fault activity. The following qualitative features of the mountain front have been also taken into account, as required for such classifications:

(i) Shape of the cross-valley profile: U-shaped valley indicates less activity than V-shaped ones. In our case, the valleys have soft V shapes, indicating active tectonics.

(ii) Piedmont landforms: development of alluvial fan systems and their size; connexion of fan channels to axial fluvial systems; channel incision. Alluvial fans developed from the mountain front are mostly short. Along the mountain front, only the main streams (those showing a catchment area broadly entering the upthrown block) are incised on alluvial fans. Short gullies, instead of being incised, suddenly split into several shallow channels and disappear as they attain fan apexes, so they are not connected with the axial fluvial system.

(iii) Development and conservation of tectonic landforms. Along the central sector of the mountain front, clear triangular facets, typical active tectonics forms, are well preserved.

The ensemble of quantitative and qualitative parameters described below allows us to apply the aforementioned classifications of fault activity, as summarized in Table 4. According to McCalpin [7], the Concud fault belongs to class 2 (‘rapid’ fault), although some features are also within the range of class 3 (‘slow’ fault). According to Silva *et al*. [8], the fault shows features of class 1 (‘active tectonics’) and, to a lesser extent, of class 2 (‘moderate tectonics’).

Both classifications empirically assign characteristic slip rates to each class. According to estimates based on McCalpin’s classification, our fault should have a slip rate comprised between 0.05 and 0.5 mm/y. According to Silva *et al*. [8] estimates, the slip rate of the Concud fault should be higher than 0.03 mm/y, and could exceed 0.08 mm/y. These values agree with our actual slip rates calculated from offset geologic markers (0.07-0.33 mm/y).

5. Discussion

The geomorphic indices and other landscape features of the Concud mountain front are comparable to those described within other tectonically active regions of the Iberian Peninsula and other countries, both in extensional and compressive settings.

Values of sinuosity index S_{mf} measured at the Concud fault escarpment (S_{mf} = 1.17-1.32; S_{mf} = 1.24 for the whole mountain front) are similar to those calculated by Perea [42] for twenty fault-generated mountain fronts at the neighbouring Maestrat grabens, eastern Iberian Chain (S_{mf} = 1.04-1.60; mean = 1.27). They also resemble those obtained at well-known active faults of the Betic Chains (SE Spain), such as the Carboneras, Lorca-Alhama or Baza faults, in which S_{mf} usually ranges from 1.05 to 1.4 [8, 43].

Values of the V_f index computed at gullies transverse to the Concud mountain front, at a distance of 250 m from the fault trace (V_f = 0.11-0.88; mean = 0.30), does not differ very much from some reported in the same conditions at Maestrat (V_f = 0.12-1.5; mean = 0.68 [42]), and Betic Chains: Baza fault (V_f = 0.28-0.86 [43]); Carboneras and Lorca-Alhama faults (0.38±0.18 to 0.59±0.56 [8]).

Slopes of the triangular facets at the Concud escarpment (about 23º) are within the range, but above the mean of those measured by Perea [42] at the Maestrat grabens and El Camp mountain front (Catalonian Ranges). This author demonstrates the positive correlation between the mean slope of facets and their absolute height differences between the toe and the peak, mainly in the case of facets modelled on limestones and dolostones (same lithology as in the Concud area). If we select facets described by Perea [42] that have similar heights to those of the Concud facets (60-100 m), most of them show slope angles comprised between 13º and 22º (exceptionally, up to 28º; mean = 19º). Slope of the Concud facets also exceeds those than could be extrapolated from height-slope statistical relationships obtained by Petit *et al*. [44, 45] using numerical models (8 to 10º for facets 60 to 100 m high). Nevertheless, these numerical models successfully account for the relationship between total height of our facets and slip rate, since they predict a throw rate of ca. 0.07-0.12 mm/y for the Concud fault.

We have already mentioned the similitude between the spacing ratio of drainage outlets at the Concud mountain front (1.97) and those reported for numerous regions of the world [34, 35, 36]. Within the Iberian Peninsula, our value is comparable, although slightly lower, to those calculated by Perea [42] at the Maestrat mountain fronts (1.39-3.85, mean = 2.22) and El Camp (1.89-2.38). It is also lower than those published for the Amer and Banyoles faults (eastern Pyrenees), which range from 1.89 to 3.85 (mean = 2.33) [42, 46]. This broadly suggests that the drainage pattern on the Concud mountain front has not been controlled by tectonic uplift as strongly has other similar active faults reported in the literature.

The observed patterns of variation of *SL* index (not considered within fault activity classifications) also fit those described in gullies crossing other active faults in the eastern Iberian Peninsula. A continuous downstream increase of 'basal' *SL* values is also reported by Salvador and Simón [47] in gullies crossing Plio-Pleistocene faults of the Alcalà de Xivert graben (Maestrat, eastern Iberian Chain), as well as by García-Tortosa *et al*. [43] in the Baza fault (Betics). Moreover, the absolute 'basal' *SL* values attained near the Concud fault, at distances of 400 to 1500 m from the drainage divide (*SL* = 40 to 80 m), approach those reported for other structures at the same positions: *SL* = 40 to 100 m at the Alcalà de Xivert graben [47]; *SL* = 30 to 70 m, in average, at the Baza fault [43].

Plotting S_{mf} vs. V_f values on the diagram proposed by Silva *et al*. [8] allows us to assess the relative position of the Concud fault among extensional fault-generated mountain fronts of eastern Spain (Fig. 9). Our low values of both S_{mf} and V_f indices represent a morphotectonic signal similar to that of extensional faults studied by Silva *et al*. [8] in the Betic Chains and Valencia area, whose S_{mf}-V_f relationship draws the tendency curve plotted in Fig. 9 (curve 1a in fig. 6 of Silva *et al*. [8]). The position of our geomorphic indices on that diagram: (i) demonstrates that the Concud fault fits the same tendency, and (ii) corroborates that it lies within the Class 1 of activity. Besides, the Concud mountain front shows similar S_{mf}-V_f values to those of most mountain fronts in the neighbouring Maestrat region, although broadly suggesting a higher level of activity than the latter (confirmed by the higher slope of triangular facets). A number of cases among the Maestrat mountain fronts that exhibit anomalously low S_{mf} values irrespective of their V_f ones (Atzeneta, Tirig, La Salzedella, Les Coves de Vinromà, Val d'Àngel) can be very probably explained by differential erosion of the Plio-Pleistocene sedimentary infill, which produce a fault-line scarp.

The possibility that geomorphic indexes of the mountain front could have been influenced by non-tectonic processes and landscape conditions, resulting in a certain overestimate of tectonic activity, should also be considered for the Concud fault. Mountain fronts in the Basin and Range, on which the usual criteria for assessment of fault activity are mostly based [5, 6, 7], are associated with alluvial fan piedmonts dominated by aggradation. This is generally the case of the Betic mountain fronts as well. In contrast, although aggradation dominated the Concud piedmont during the Late Pleistocene (alluvial fans dated between **77** ± 4 ka and 20 ± 1 ka), episodes of significant base level drop and subsequent downcutting of the drainage network took place by Early, Middle Pleistocene and Holocene times. Those occurring after alluvial fan building apparently had not significant influence, since the overall pediment morphology has been kept from the most recent fluvial incision. Nevertheless, those occurring before probably contributed to rejuvenation of the Concud mountain front in association with fault activity. These circumstances should be taken into account when geomorphic and geologic evidences of fault activity are compared, and probably explain why the application of McCalpin's classification leads to overestimate the slip rate (up to 0.5 mm/y) of the Concud fault.

Independently on its geomorphologic expression, the slip rate at the extensional Concud fault is well constrained from geologic markers: 0.07 to 0.10 mm/y since mid Pliocene times; 0.08 to 0.33 mm/y, according to different approaches and dating hypothesis, since mid Pleistocene. Such rates are comparable to those calculated for: (i) the Munébrega normal fault, at the central Iberian Chain (0.10 mm/y [48]); (ii) normal faults of the Betic Chains, as the Granada (0.03-0.38 mm/y [49]), Ventas de Zafarraya (0.3-0.45 mm/y during Holocene times [50]), or Baza fault (0.12-0.33 mm/y [43, 51]); (iii) throw component of strike-slip faults of the Betic Chains, e.g. Lorca-Alhama (0.04-0.35 [8, 52, 53]) or Carboneras (0.08-0.1 mm/y [8]); (iv) some moderately active normal faults at south-western U.S.A., as the frontal Sierra Nevada (0.2-0.3 mm/y [54]), Río Grande (0.1-0.36 mm/y [7]), Dixie Valley (0.2-0.5 mm/y [55]), or Pajarito fault (0.1 mm/y [56]); (v) other 'second level' normal faults all around the world, e.g. Irpinia fault (Italy; 0.3 mm/y [57]), faults bounding the Denizly graben-horst system (Turkey; 0.15 mm/y [58]), or Taupo rift (New Zealand; 0.30-0.34 mm/y [59]). In contrast, the Concud fault moves at higher rates than El Camp fault (0.02-0.08 mm/y [60, 61]), and most faults of eastern Maestrat (0.02-0.10 mm/y [62]).

Perhaps, the Concud fault could appear as anomalously rapid seeing at its regional tectonic and seismic framework (overall gentle deformation and very low instrumental seismicity). It may be difficult to assume that their slip rates are similar to those calculated at extensional faults of a much more active region as the Betic Chains. The reason probably deals with the particular tectonic position and role of the Concud fault. While at southeastern Betics the total crustal deformation is distributed among a number of large faults, no other fault at the central-eastern Iberian Chain has any evidence of continuous activity during Middle-Late Pleistocene times comparable to the Concud fault. Regional deformation during the Plio-Pleistocene transition was widely distributed among several tens of faults at a macrostructural scale; in contrast, along Pleistocene times, deformation seems to have been progressively concentrated into a few inland faults, while structures located near the coast became quiescent. The same tendency has been observed e.g. in central Apennines (Italy) since 0.9 Ma [63]. Therefore, we can hypothesize that the Concud fault accommodates most of the total crustal extension at this sector of the Iberian Chain, which could explain the apparently anomalous inferred slip rates.

6. Conclusions

Qualitative and quantitative geomorphic features of the mountain front and the piedmont associated to the Concud fault are in agreement with slip rates inferred from stratigraphic markers. Moreover, the results approach those obtained in similar active normal faults within the Iberian Peninsula and other regions of the world.

The extensional Concud fault has been active during Late Pliocene and Pleistocene times, producing a maximum net displacement in the range of 240 m to 360 m and giving rise to a 60 to 120 m-high mountain front. Slip rates ranging from 0.07 to 0.33 mm/y have been calculated from geological evidences (offset of well dated stratigraphic markers, Late Pliocene to Late Pleistocene in age).

Following another independent approach, values of geomorphic indices (valley width/height ratio, V_f, and mountain-front sinuosity, S_{mf}), as well as other qualitative landscape features, have been introduced into classifications of fault activity. The results indicate a ‘moderate’ to ‘active’ (according to Silva *et al*. [8]), or even a ‘rapid’ (according to McCalpin [7] activity, which could be estimated, in terms of slip rate, in the range of 0.03 to 0.5 mm/y, therefore enclosing the range of slip rates inferred from stratigraphic markers. Stream-gradient index (*SL*), calculated along a number of gullies that cross the mountain front, have not been used for those classifications; however, the anomalously high values found close (upstream) to the Concud fault trace corroborate the occurrence of significant tectonic activity.

Morphometric analysis of landforms and drainage networks induced or modified by active faults constitutes a useful approach to their level of activity. Our comparative study at the Concud fault gives shows a reasonable consistence with classifications proposed by Bull and McFadden [5], McCalpin [7] and Silva *et al*. [8], which could therefore considered as a functional implement for approaching fault slip rates in the studied region (central-eastern Iberian Chain). Nevertheless, assessment of fault activity should take into account the particular geomorphic setting of each region. The aforementioned classifications are based on data of mountain fronts mostly associated to alluvial piedmonts dominated by aggradation, whereas the Concud piedmont has undergone episodes of base level drop that probably contributed to rejuvenation of the mountain front and could give the impression of a somehow higher level of activity. In particular, the highest potential slip rate derived from McCalpin’s classification (0.5 mm/y) clearly represents an overestimate.

We can not compare the entire results of the present study with other faults of the Iberian Chain, since the Concud fault is the only one in which both geomorphic indices and precise slip rates inferred from geologic markers have been reported. Nevertheless, our results suggest that, at least for the Late Pleistocene, its level of activity is analogous to that of normal faults of the Betic Chains, and of some moderately active, ‘second order’ normal faults at south-western U.S.A. and other regions of the world. In contrast, it seems to be higher than most extensional faults of other regions at the north-western margin of the Valencia Trough (Valencia, Maestrat, Catalonian Ranges). This relatively high level of activity within its regional tectonic and seismic framework is probably due to the fact that the Concud fault has accommodated most of the total crustal extension at this sector of the Iberian Chain during Late Pleistocene times.

Acknowledgements

The research has been financed by projects CGL2009-13390 and Consolider CGL2006-041 (*Topo-Iberia*) of Spanish Ministerio de Ciencia e Innovación - FEDER, as well as by the Aragón regional government (Geotransfer research group). The topographical profile of Fig. 4c is based on a levelling survey made in collaboration with A. Calvo Cases. Our research benefited from data and comments by H. Perea about geomorphic indices of the Maestrat mountain fronts. L.E. Arlegui and C.L. Liesa helped us with geological and paleoseismological studies leading to calculate slip rates from stratigraphic markers.

References

[1] Keller, E.A., Investigation of active tectonics: use of surficial Earth processes, in: Wallace, R.R. (Ed.), Active Tectonics: Impact on Society, National Academic Press, Washington, 1986, pp. 136-147.

[2] Burbank, D.W., Anderson, R.S., Tectonic Geomorphology, Wiley-Blackwell, Oxford, 2012, 454 p.

[3] Merrits, D.J., Vincent, K.R., Geomorphic response of coastal streams to low, intermediate and high rates of uplift, Mendocino triple junction region, northern California, Geol. Soc. Am. Bull. 101 (1989) 1373-1388.

[4] Hack, J.T., Stream profile analysis and stream-gradient index, U.S. Geol. Surv. J. Res. 1 (1973) 421-429.

[5] Bull, W.B., McFadden, L.D., Tectonic Geomorphology north and south of the Garlock fault California, in: Doehring, D.O. (Ed.), Geomorphology in arid regions, Allen & Unwin, London, 1977, pp. 115-138.

[6] Bull, W.B., Geomorphic tectonic activity classes of the south front of the San Gabriel Mountains, California, U.S. Geological Survey Contract Report 14-08-001-G-394, Office of Earthquakes, Volcanoes and Engineering, Menlo Park, California, 1978, 59 p.

[7] McCalpin, J.P., Paleoseismology, Academic Press, London, 1996, 588 p.

[8] Silva, P.G., Goy, J.L., Zazo, C., Bardají, T., Fault-generated mountain fronts in southeast Spain: geomorphologic assessment of tectonic and seismic activity, Geomorphology 50 (2003) 203-225.

[9] Rockwell, T.J., Keller, E.A., Johnson, D.L., Tectonic Geomorphology of alluvial fans and

mountain fronts near Ventura, California, in: Morisawa, M., Hack, J.T. (Eds.), Tectonic Geomorphology, Allen & Unwin, Boston, 1985, pp. 183-207.

[10] Simón, J.L., Lafuente, P., Arlegui, L.E., Liesa, C.L., Soriano, M.A., Caracterización paleosísmica preliminar de la falla de Concud (fosa del Jiloca, Teruel), Geogaceta 38 (2005) 63-66.

[11] Lafuente, P., Arlegui, L.E., Liesa, C.L., Simón, J.L., Nuevo estudio paleosismológico en el sector central de la falla de Concud (Fosa del Jiloca, Teruel): resultados preliminares, 1ª Reunión Ibérica sobre Fallas Activas y Paleosismología, Sigüenza (Guadalajara, Spain), 2010, pp. 67-70.

[12] Lafuente, P., Arlegui, L.E., Liesa, C.L., Simón, J.L., Paleoseismological analysis of an intraplate extensional structure: the Concud fault (Iberian Chain, Spain), Int J Earth Sci (Geol Rundsch), 100 (2011) 1713-1732.

[13] Lafuente, P., Arlegui, L.E. y Liesa, C.L., Simón, J.L. (2011b). Reply to the discussion by F. Gutiérrez, P. Lucha, J. Guerrero, M. Gutiérrez and D. Carbonel on the article 'Paleoseismological analysis of an intraplate extensional structure: the Concud fault (Iberian Chain, eastern Spain)'. Int J Earth Sci (Geol Rundsch) (2011) DOI 10.1007/s00531-011-0661-3.

[14] Lafuente, P., Tectónica activa y paleosismicidad de la falla de Concud (Cordillera Ibérica central), Thesis Universidad de Zaragoza, 2011, 253 p. + annexes.

[15] Simón, J.L., Compresión y distensión alpinas en la Cadena Ibérica Oriental, Thesis Universidad de Zaragoza (1982), Publ. Inst. Estudios Turolenses, Teruel, 1984, 269 p.

[16] Simón, J.L., Tectónica y neotectónica del sistema de fosas de Teruel, Teruel 69 (1983) 21-97.

[17] Roca, E., Guimerà, J., The Neogene structure of the eastern Iberian margin: structural constraints on the crustal evolution of the Valencia trough (western Mediterranean), Tectonophysics 203 (1992) 203-218.

[18] Godoy, A., Ramírez, J.I., Olivé, A., Moissenet, E., Aznar, J.M., Aragonés, E., Aguilar, M.J., Ramírez del Pozo, J., Leal, M.C., Jerez-Mir, L., Adrover, R., Goy, A., Comas, M.J., Alberdi, M.T., Giner, J., Gutiérrez-Elorza, M., Portero, J.M., Gabaldón, V., Mapa Geológico de España 1: 50.000, hoja nº 567 (Teruel), IGME, Madrid, 1983.

[19] Alcalá, L., Alonso-Zarza, A.M., Álvarez, M.A., Azanza, B., Calvo, J.P., Cañaveras, J.C., van Dam, J.A., Garcés, M., Krijgsman, W., van der Meulen, A.J., Morales, J., Peláez, P., Pérez-González, A., Sánchez, S., Sancho, R., Sanz, E., El registro sedimentario y faunístico de las cuencas de Calatayud-Daroca y Teruel. Evolución paleoambiental y paleoclimática durante el Neógeno, Rev. Soc. Geol. España 13 (2000) 323-343.

[20] Simón, J.L., Late Cenozoic stress field and fracturing in the Iberian Chain and Ebro Basin (Spain), J. Struct. Geol. 11 (1989) 285-294.

[21] Arlegui, L.E., Simón, J.L., Lisle, R.J., Orife, T., Late Pliocene-Pleistocene stress field in the Teruel and Jiloca grabens (eastern Spain): contribution of a new method of stress inversion, J. Struct. Geol. 27 (2005) 693-705.

[22] Rubio, J.C., Simón, J.L., Tectonic subsidence v. erosional lowering in a controversial intramontane depression: the Jiloca basin (Iberian Chain, Spain), Geol. Mag. 144 (2007) 1-15.

[23] Moissenet, E., Le Quaternaire moyen alluvial du fossé de Teruel (Espagne), Physio-Géo 14/15 (1985) 61-78.

[24] Gutiérrez, F., Gutiérrez, M., Gracia, F.J., McCalpin, J.P., Lucha, P., Guerrero, J., Plio-Quaternary extensional seismotectonics and drainage network development in the central sector of the Iberian Range (NE Spain), Geomorphology 102 (2008) 21-42.

[25] Peña, J.L., Las acumulaciones cuaternarias de la confluencia de los ríos Alfambra y Guadalaviar en las cercanías de Teruel, Actas VII Col. Geografía, Pamplona, 1981, pp. 1-13.

[26] Sánchez Fabre, M., Estudio geomorfológico de la Depresión de Alfambra-Teruel-Landete y sus rebordes montañosos, Thesis Universidad de Zaragoza, 1989, 926 p.

[27] Moissenet, E., L'age et les déformations des terrases alluviales du Fossé de Teruel, in: El Cuaternario de España y Portugal, IGME-AEQUA, Madrid, 1, 1993, 267-279.

[28] Santonja, M., Moissenet, E., Pérez-González, A., Villa, P., Sesé, C., Soto, E., Eisenmann, V., Mora, R., Dupré, M., Cuesta de la Bajada: un yacimiento del Pleistoceno Medio en Aragón, Arqueol. Aragonesa 21 (1994) 61-68.

[29] Arlegui, L.E., Simón, J.L., Lisle, R.J., Orife, T., Analysis of non-striated faults in a recent extensional setting: the Plio-Pleistocene Concud fault (Jiloca graben, eastern Spain), J. Struct. Geol. 28 (2006) 1019-1027.

[30] Opdyke, N., Mein, P., Lindsay, E., Pérez-González, A., Moissenet, E., Norton, V.L., Continental deposits, magnetostratigraphy and vertebrate paleontology, late Neogene of Eastern Spain, Palaeogeogr., Palaeoclimatol., Palaeoecol. 133 (1997) 129-148.

[31] Wallace, R.E., Profiles and ages of young fault scarps, north-central Nevada, Geol. Soc. Am. Bull. 88 (1977) 1267-1281.

[32] Mayer, L., Tectonic geomorphology of the escarpments and mountain fronts, in: Wallace, R.E. (Ed.), Active Tectonics: Impact on Society, National Academic Press, Washington, 1986, pp. 125-135.

[33] Wallace, R.E., Geometry and rates of change of fault-generated range fronts, north-central

Nevada, Journal of Research of the United States Geological Survey, 6 (1978) 637-650.

[34] Hovius, N., Regular spacing of drainage outlets from linear mountain belts, Basin Research 8 (1996) 29-44.

[35] Talling, P.J., Stewart, M.D., Stark, C.P., Gupta, S., Vincent, S.J., Regular spacing of drainage outlets from linear fault blocks, Basin Research 9 (1997) 275-302.

[36] Walcott, R.C., Summerfield, M.A., Universality and variability in basin outlet spacing: implications for the two-dimensional form of drainage basins, Basin Research 21 (2009) 147-155.

[37] Keller, E.A., Rockwell, T.K., Tectonic geomorphology, Quaternary chronology and paleoseismicity, in: Costa, J.E., Fleisher, P.J. (Eds), Development and Applications of Geomorphology, Springer, Berlin, 1984, pp. 203–239.

[38] Seeber, L., Gornitz, V., River profiles along the Himalayan arc as indicators of active tectonics. Tectonophysics 92 (1983) 335-367.

[39] Regional Government of Aragón, Spain, http://sitar.aragon.es/

[40] Yeats, R.S., Sieh, K., Allen, C.R., The Geology of Earthquakes, Oxford University Press, New York, 1997, 568 p.

[41] Wells, S.G., Bullard, T.F., Menges, C.M., Drake, P.G., Karas, P.A., Kelson, K.I., Ritter, J.B., Wesling, J.R., Regional variations in tectonic geomorphology along a segmented convergent plate boundary pacific coast of Costa Rica, Geomorphology 1 (1988) 239-265.

[42] Perea, H., Falles actives i perillositat sísmica al marge nord-occidental del solc de Valencia. Thesis Universitat de Barcelona (2006) 317 p.

[43] García-Tortosa, F.J., Sanz de Galdeano, C., Sánchez-Gómez, M., Alfaro, P., Geomorphologic evidence of the active Baza Fault (Betic Cordillera, South Spain), Geomorphology 97 (2008) 374–391.

[44] Petit, C., Meyer, B., Gunnell, Y., Jolivet, M., San'kov, V., Strak, V., Gonga-Saholiariliva, N., Height of faceted spurs, a proxy for determining long-term throw rates on normal faults: Evidence from the North Baikal Rift System, Siberia. Tectonics 28 (2009) doi:10.1029/2009TC002555.

[45] Petit, C., Gunnell, Y., Gonga-Saholiariliva, N., Meyer, B., Seguinot, J., Faceted spurs at normal fault scarps: Insights from numerical modeling, Journal of Geophysical Research-Solid Earth 114 (2009) doi:10.1029/2008JB005955.

[46] Ferrer, P., Masana, E., Santanach, P., Expresión geomorfológica de la actividad reciente de la falla de Amer (NE de la Península Ibérica), Acta Geol. Hispánica 31 (1999) 17-24.

[47] Salvador, T., Simón, J.L., Un ejemplo de valles decapitados en las fosas cuaternarias del Maestrazgo (Castellón). Actas I Reunión Nacional de Geomorfología, Teruel, 1990**,** pp. 61-70.

[48] Gutiérrez, F., Masana, E., González, A., Lucha, P., Guerrero, J., McCalpin, J., Late Quaternary paleoseismic evidence on the Munébrega half-graben fault (Iberian Range, Spain), Int. J. Earth Sci. (2008) DOI: 10.1007/s00531-008-0319.

[49] Sanz de Galdeano, C., Peláez, J.A., López-Casado, C., Seismic potential of the main active faults in the Granada Basin (Southern Spain), Pure Appl. Geophys. 160 (2003) 1537-1556.

[50] Reicherter, K., Jabaloy, A., Galindo-Zaldívar, J., Becker-Heidmann, P., Sanz de Galdeano, C., Trenching results of the Ventas de Zafarraya fault (Southern Spain). 1ª Reunión Ibérica sobre Fallas Activas y Paleosismología, Sigüenza (Guadalajara, Spain), 2010, p. 125.

[51] Alfaro, P., Delgado, J., Sanz de Galdeano, C., Galindo-Zaldívar, J., García-Tortosa, F.J., López-Garrido, A.C., López-Casado, C., Marín, C., Gil, A., Borque, M.J., The Baza Fault: a major active extensional fault in the Central Betic Cordillera (South Spain). Int. J. Earth Sci. (2008) doi:10.1007/s00531-007-0213-z.

[52] Martínez-Díaz, J.J., Masana, E., Hernández-Enrile, J.L. y Santanach, P., Evidence for seismic events of recurrent prehistoric deformation along the Alhama de Murcia fault, southeastern Spain, Acta Geol. Hispanica 36 (2001) 315-327.

[53] Masana, E., Martínez-Díaz, J. J., Hernández-Enrile, J. L., Santanach, P., The Alhama de Murcia fault (SE Spain), a seismogenic fault in a diffuse plate boundary: Seismotectonic implications for the Ibero-Magrebian region, J. Geophys. Res. 109 (2004) B01301, doi:10.1029/2002JB002359.

[54] Le, K., Lee, J., Owen, L. A., Finkel, R., Late Quaternary slip rates along the Sierra Nevada frontal fault zone, California: Slip partitioning across the western margin of the Eastern California Shear Zone–Basin and Range Province, GSA Bull. (2006) doi: 10.1130/B25960.

[55] Bell, J.W. y Katzer, T., Timing of the late Quaternary faulting in the 1954 Dixie valley earthquake area, Central Nevada, Geology 18 (1990) 622-625.

[56] McCalpin, J. P., Late Quaternary activity of the Pajarito fault, Rio Grande rift of northern New Mexico, USA, Tectonophysics 408 (2005) 213– 236.

[57] Pantosti, D., Valensise, G. Faulting mechanism and complexity of the November 23, 1980, Campania-Lucania earthquake, inferred from surface observations, J. Geophys. Res. 95 (1990) 15319-15341.

[58] Koçyigit, A., The Denizli graben-horst system and the eastern limit of western Anatolian continental extenion: basin fill, structure, deformational mode, throw amount and episodic

evolutionary history, SW Turkey, Gedinamica Acta 18 (2005) 167-208.

[59] Canora-Catalán, C., Villamor, P., Berryman, K., Martínez-Díaz, J.J., Raen, T., Rupture history of the Whirinaki fault, an active normal fault in the Taupo rift, New Zealand, New Zealand Journal of Geology and Geophysics 51 (2010) 277-293.

[60] Masana, E., Villamarin, J.A., Santanach, P., Paleoseismic results from multiple trenching analysis along a silent fault: The El Camp fault (Tarragona, northeastern Iberian Peninsula), Acta Geol. Hispanica 36 (2001) 329-354.

[61] Perea, H., Masana, E., Santanach, P., A pragmatic approach to seismic parameters in a region with Low Seismicity: the case of eastern Iberia, Natural Hazards 39 (2006) 451–477.

[62] Simón, J.L., Arlegui, L.E., Lafuente, P. y Liesa, C.L., Active extensional faults in the central-eastern Iberian Chain, Spain. *Iberian Geology* 38 (2012) 133-152.

[63] Roberts, G.P., Michetti, A.M., Cowie, P., Nigel C. Morewood, N.C., Papanikolaou, I., Fault slip-rate variations during crustal-scale strain localisation, central Italy. Geophysical Research Letters, 29 (2002) doi: 1168, 10.1029/2001GL013529.

FIGURE CAPTIONS

Figure 1. Geological map of the Jiloca and Teruel grabens showing location of the study area. Inset: location within the Iberian Peninsula.

Figure 2. Geological map of the Concud fault (see location in Fig. 1).

Figure 3. Cross sections of the Concud fault allowing to calculate slip rates for distinct recent geologic time lapses. (a) Offset of mid-Pliocene lacustrine deposits. (b) Offset of a Middle-Pleistocene fluvial terrace at Los Baños site. (c) Offset of a Late Pleistocene pediment at El Hocino site. See text for references of ages.

Figure 4. (a) Digital elevation model of the studied area, showing the drainage network and drainage basins (numbered for references in text). (b) Detailed geomorphologic map of a sector of the fault-generated mountain front and its piedmont (see location on a).

Figure 5. (a) Field view of triangular facets. (b) Transverse topographic profile of the central facet in (a).

Figure 6. (a) Longitudinal profiles of seventeen gullies transverse to the Concud mountain front (see location in Fig. 4a). Vertical exaggeration: 2X. *K* (*gradient index* of the entire profile) = $\Delta H_T / ln\ L_T$, where H_T is the total height difference, and L_T is the total length. (b) Variation of the Stream-gradient index (*SL*, scale on the left) and the corresponding *SL/K* ratio (scale on the right) for the same gullies. An arbitrary value $SL/K = 5$ has been marked as a threshold for filtering significant profile anomalies (segments identified by thick traces on profiles). Sloping thick dashed lines: basal tendency of the *SL* curves; vertical thick dashed lines: position of the fault traces. Open dots above maxima: *SL* anomalies related to bed-rock lithology; solid triangles above maxima: *SL* anomalies interpreted as related to tectonic uplift.

Figure 7. Up: Values of the Valley width/height ratio (V_f) calculated for a number of transverse gullies at 250 m and 500 m upstream from the fault trace. Down: Two examples of cross-valley profiles at those positions (gullies 8 and 13).

Figure 8. Trace of the mountain-piedmont junction used for calculating the Mountain-front sinuosity index (S_{mf}). A-B and C-D: lithologically-defined segments in which S_{mf} values have been calculated separately.

Figure 9. Plot of S_{mf} vs. V_f values (as proposed by Silva *et al*. [8]), showing the relative position of the Concud fault among extensional fault-generated mountain fronts of eastern Spain. Class 1, 2, 3: activity classes (active, moderate and inactive, respectively). The curve represents the tendency or regression line observed by Silva *et al*. [8] for normal faults in SE Spain.

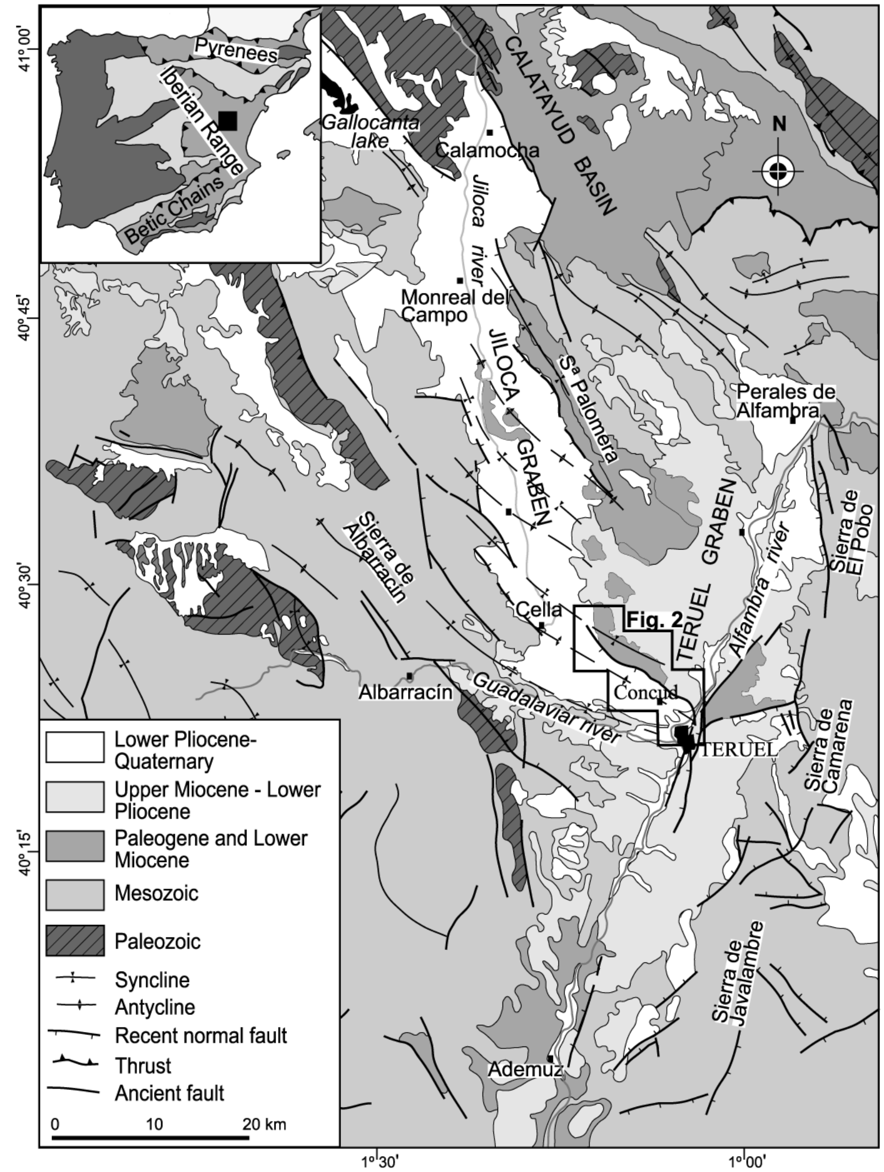

Figure 1. Geological map of the Jiloca and Teruel grabens showing location of the study area. Inset: location within the Iberian Peninsula.

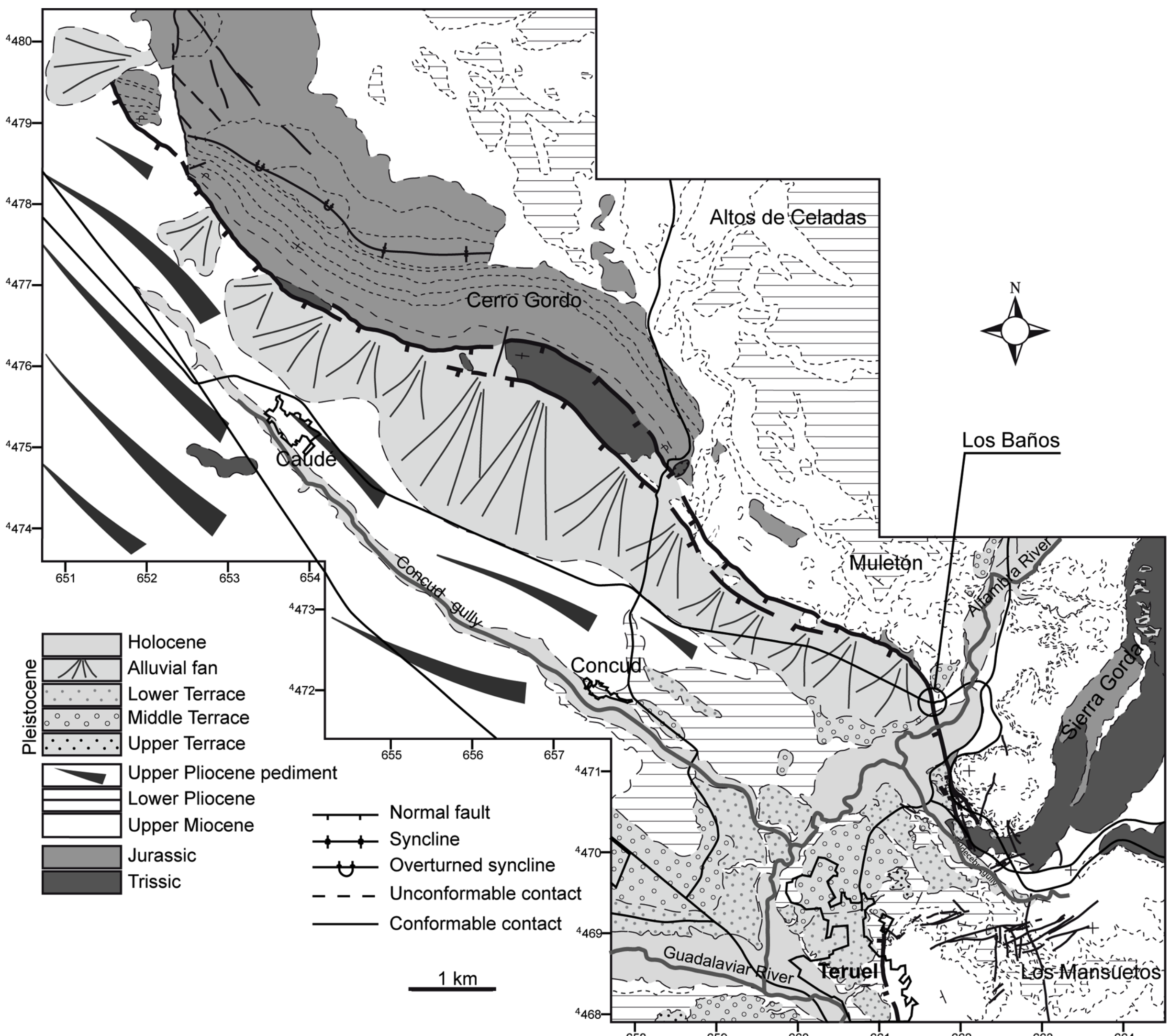

Figure 2. Geological map of the Concud fault (see location in Fig. 1).

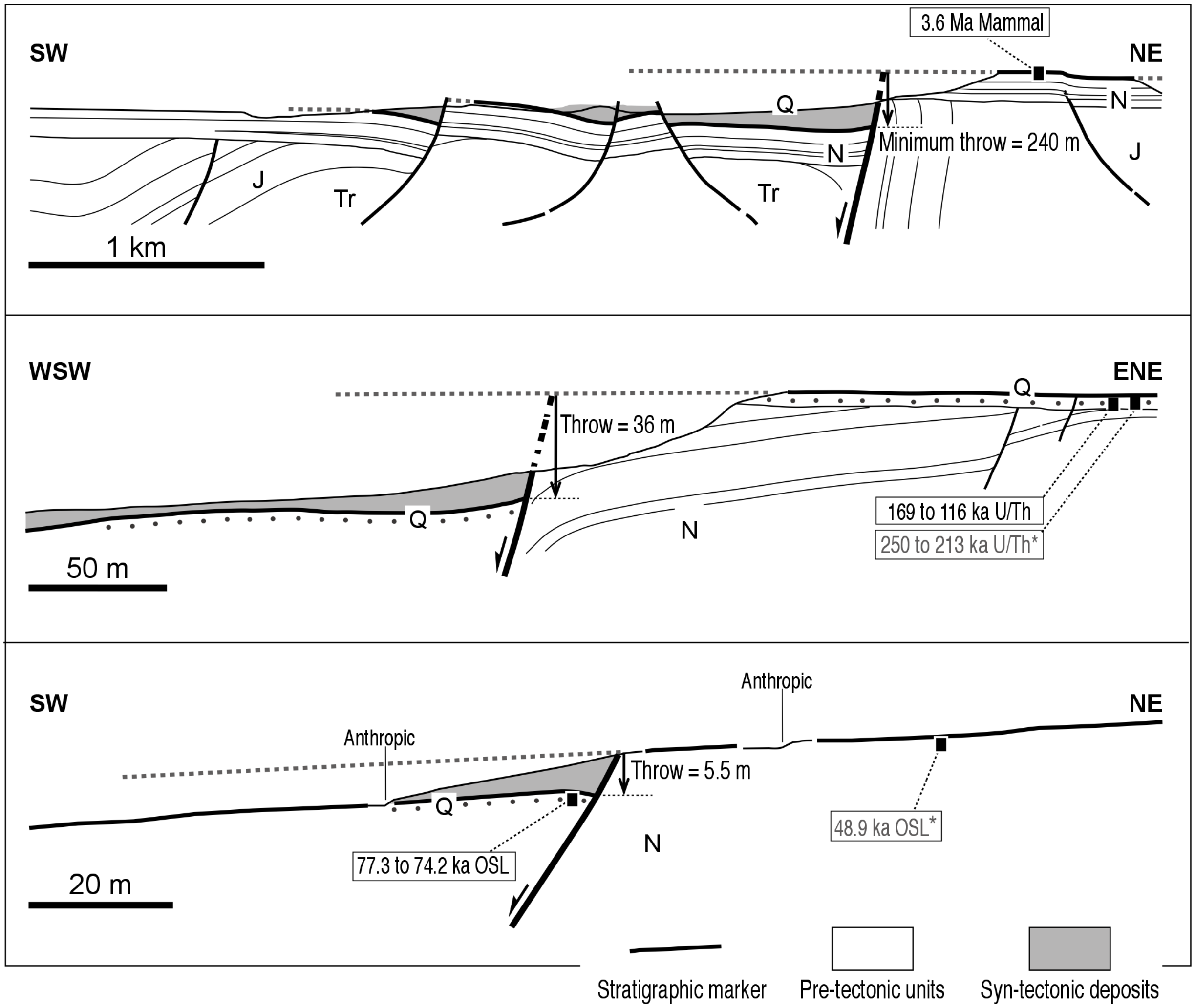

Figure 3. Cross sections of the Concud fault allowing to calculate slip rates for distinct recent geologic time lapses. (a) Offset of mid-Pliocene lacustrine deposits. (b) Offset of a Middle-Pleistocene fluvial terrace at Los Baños site. (c) Offset of a Late Pleistocene pediment at El Hocino site. See text for references of ages.

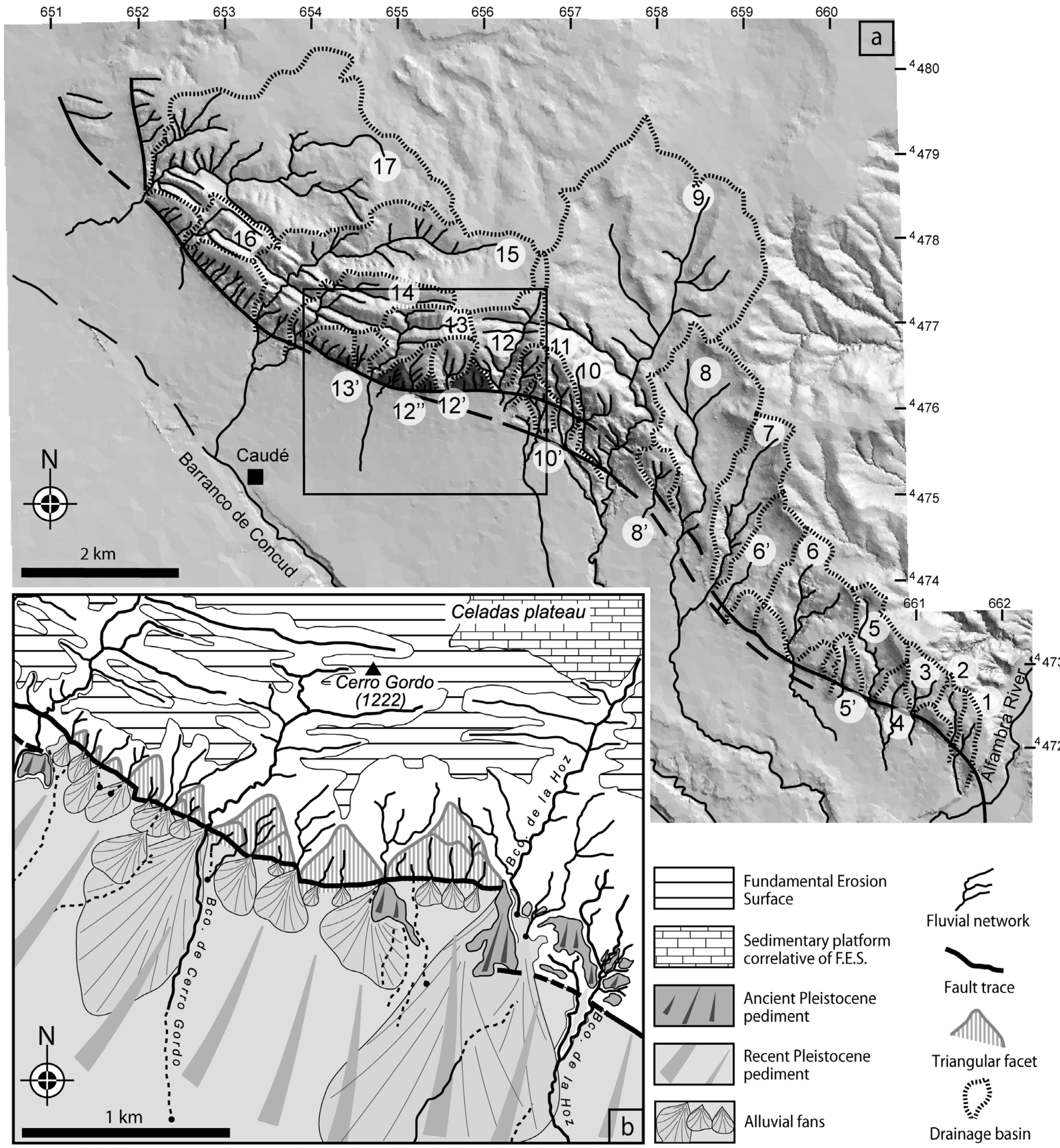

Figure 4. (a) Digital elevation model of the studied area, showing the drainage network and drainage basins (numbered for references in text). (b) Detailed geomorphologic map of a sector of the fault-generated mountain front and its piedmont (see location on a).

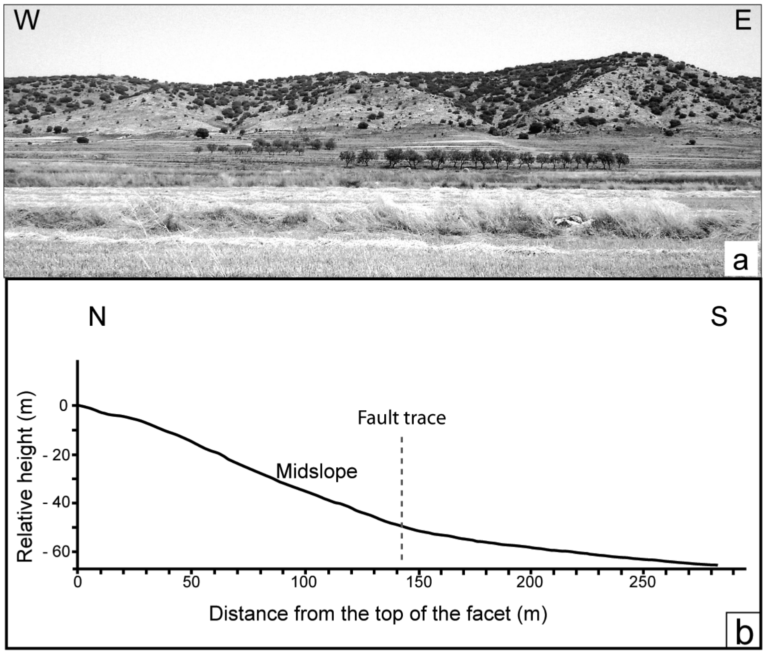

Figure 5. (a) Field view of triangular facets. (b) Transverse topographic profile of the central facet in (a).

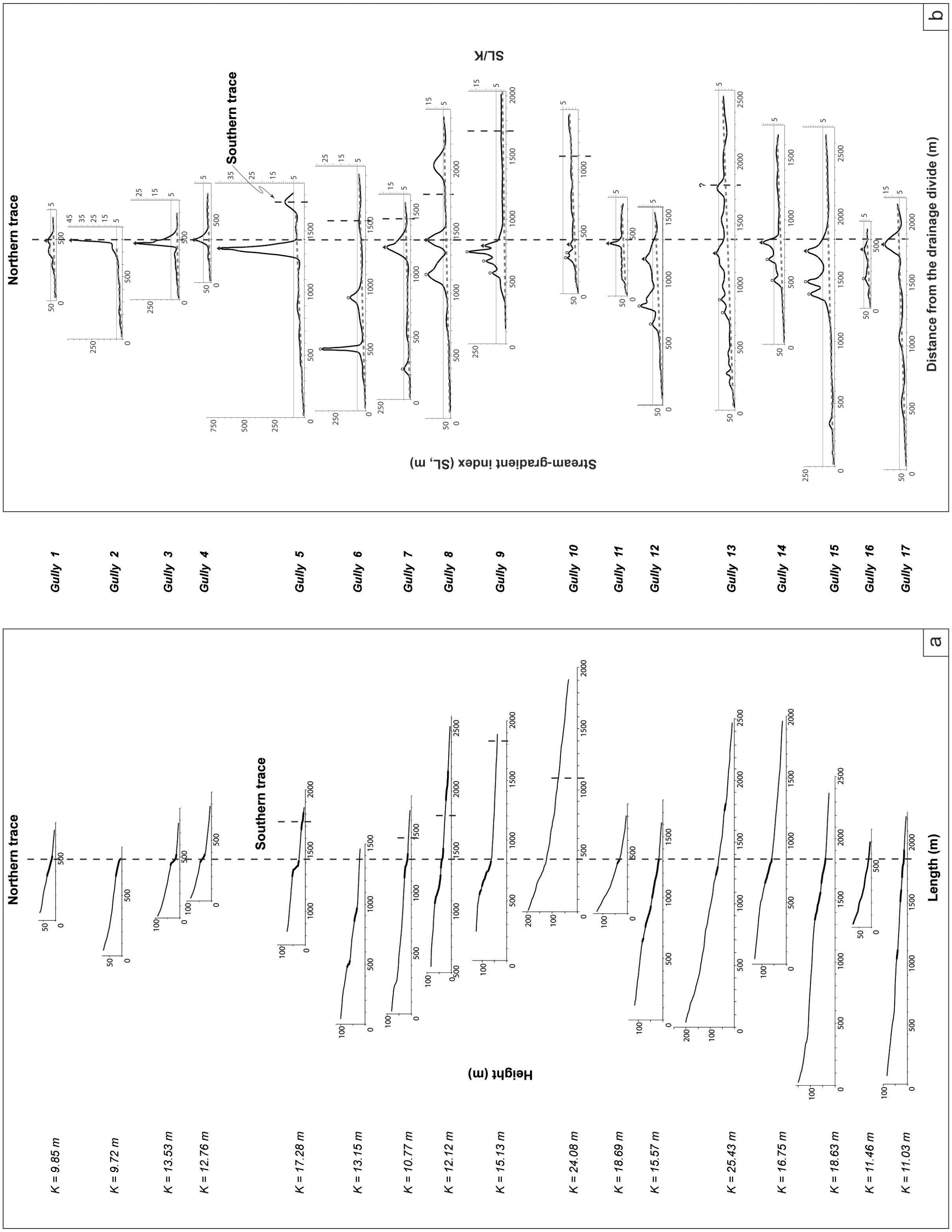
a
b
Northern trace
Southern trace
Length (m)
Height (m)
Distance from the drainage divide (m)
Stream-gradient index (SL, m)
SL/K
Gully 1
Gully 2
Gully 3
Gully 4
Gully 5
Gully 6
Gully 7
Gully 8
Gully 9
Gully 10
Gully 11
Gully 12
Gully 13
Gully 14
Gully 15
Gully 16
Gully 17
K = 9.85 m
K = 9.72 m
K = 13.53 m
K = 12.76 m
K = 17.28 m
K = 13.15 m
K = 10.77 m
K = 12.12 m
K = 15.13 m
K = 24.08 m
K = 18.69 m
K = 15.57 m
K = 25.43 m
K = 16.75 m
K = 18.63 m
K = 11.46 m
K = 11.03 m

FIG. 6

Figure 6. (a) Longitudinal profiles of seventeen gullies transverse to the Concud mountain front (see location in Fig. 4a). Vertical exaggeration: 2X. *K* (*gradient index* of the entire profile) = $\Delta H_T / ln\ L_T$, where H_T is the total height difference, and L_T is the total length. (b) Variation of the Stream-gradient index (*SL*, scale on the left) and the corresponding *SL/K* ratio (scale on the right) for the same gullies. An arbitrary value *SL/K* = 5 has been marked as a threshold for filtering significant profile anomalies (segments identified by thick traces on profiles). Sloping thick dashed lines: basal tendency of the *SL* curves; vertical thick dashed lines: position of the fault traces. Open dots above maxima: *SL* anomalies related to bed-rock lithology; solid triangles above maxima: *SL* anomalies interpreted as related to tectonic uplift.

250 m upstream	
Gully	V_f
1	0.437
2	0.389
4	0.249
5	0.244
6	0.214
7	0.213
8 (trace S)	0.497
8	0.224
9	0.231
10	0.880
11	0.419
12	0.113
13	0.140
14	0.132
15	0.155
16	0.139
17	0.362

500 m upstream	
Gully	V_f
2	0.321
6	0.265
7	0.172
8	0.212
10	0.262
12	0.060
13	0.105
14	0.098
15	0.401
17	0.159

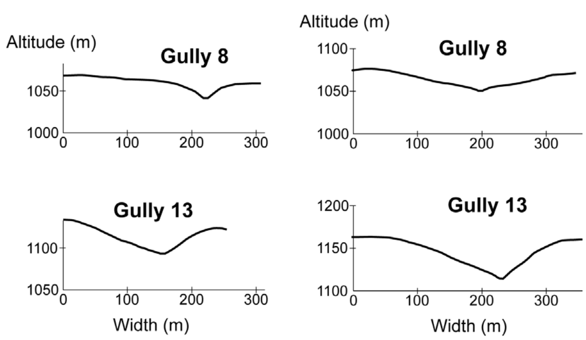

Figure 7. Up: Values of the Valley width/height ratio (V_f) calculated for a number of transverse gullies at 250 m and 500 m upstream from the fault trace. Down: Two examples of cross-valley profiles at those positions (gullies 8 and 13).

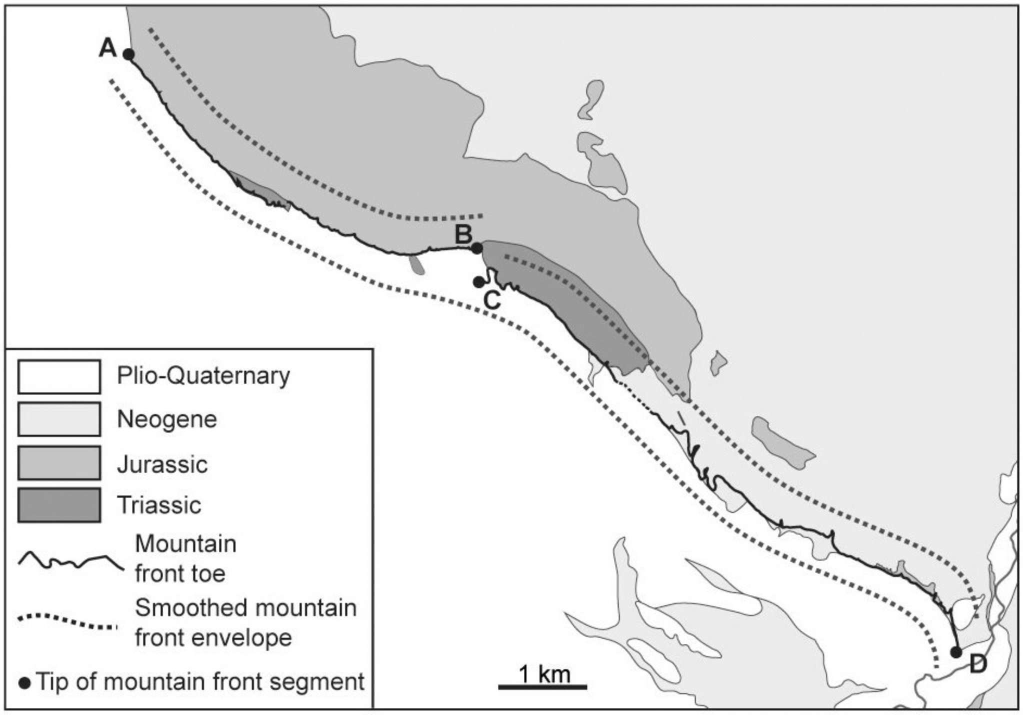

Figure 8. Trace of the mountain-piedmont junction used for calculating the Mountain-front sinuosity index (S_{mf}). A-B and C-D: lithologically-defined segments in which S_{mf} values have been calculated separately.

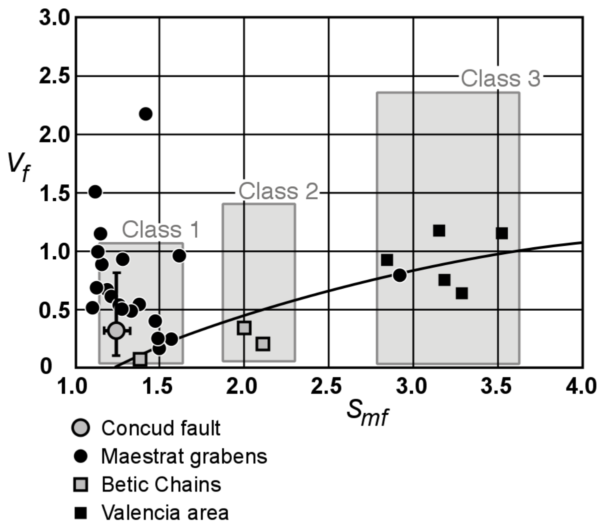

Figure 9. Plot of S_{mf} vs. V_f values (as proposed by Silva *et al*. [8]), showing the relative position of the Concud fault among extensional fault-generated mountain fronts of eastern Spain. Class 1, 2, 3: activity classes (active, moderate and inactive, respectively). The curve represents the tendency or regression line observed by Silva *et al*. [8] for normal faults in SE Spain.

TABLE CAPTIONS

Table 1. Net slip rates at the Concud fault, inferred from for different time lapses within Late Pliocene-Pleistocene times. The ratio for gullies of category III (1.97) is adequate for comparison with values published by other authors.

Table 2. Spacing ratio of drainage outlets, calculated separately for the four defined categories of transverse gullies. Distance between fault trace and drainage divide is measured orthogonal to the mountain front.

Table 3. Calculation of the Mountain-front sinuosity index (S_{mf}) with reference to both the 'straight' and the 'curved' overall length (see location sketch in Fig. 8).

Table 4. Classification of the Concud fault activity, based on quantitative and qualitative features of the fault-generated mountain front and the piedmont. Right column: parameters of the Concud fault used to classify it according to McCalpin [7] and Silva *et al*. [8]

	Overall fault	**Los Baños area (SE sector)**		**El Hocino area (central sector)**
	Post-Ruscinian	**Post-Middle Pleistocene**	**Intra-Late Pleistocene**	**Post-Late Pleistocene**
Computed time lapse	since 3.6 Ma BP	since 250-116 ka BP	since 72 ka until 32 ka	since 77-74 ka BP
Net slip (m)	250-360	39	10-12.5	6.1
Net slip rate (mm/y)	0.07-0.10	0.16-0.33	0.25-0.31	0.08

Table 1. Net slip rates at the Concud fault, inferred from for different time lapses within Late Pliocene-Pleistocene times. The ratio for gullies of category III (1.97) is adequate for comparison with values published by other authors.

	Mean distance between fault trace and drainage divide (L_b, in km)	**Mean outlet spacing (L_{os}, in km)**	**Spacing ratio: $\frac{L_b}{S_{os}}$**
Gullies category I	2.64	1.37	1.93
Gullies category II	1.36	1.11	1.23
Gullies category III	0.71	0.36	**1.97**
Gullies category IV	0.24	0.10	2.40

Table 2. Spacing ratio of drainage outlets, calculated separately for the four defined categories of transverse gullies. Distance between fault trace and drainage divide is measured orthogonal to the mountain front.

	Length of the sinuous mountain front toe (L_{mf}, km)	Straight length (L_{ss}, km)	Length of the broadly curved envelope (L_{sc}, km)	$S_{mf} = L_{mf} / L_{ss}$	$S_{mf} = L_{mf} / L_{sc}$
Whole mountain front (A-D)	14.5	11.7	12.3	**1.24**	1.18
NW segment (A-B)	5.4	4.6	5.0	**1.17**	1.08
SE segment (B-C)	9.1	6.9	7.2	**1.32**	1.26

Table 3. Calculation of the Mountain-front sinuosity index (S_{mf}) with reference to both the 'straight' and the 'curved' overall length (see location sketch in Fig. 8).

	McCalpin [7]		**Silva *et al.*** [8]		**Concud fault**
	Class 2 (‘rapid’)	**Class 3 (‘slow’)**	**Class 1 (‘active’)**	**Class 2 (‘moderate’)**	
V_f	500 m upstream from fault trace: 0.06-0.53 (mean = 0.15)	500 m upstream from fault trace: 0.2-3.5 (mean = 1.5)	250 m upstream from fault trace: < 0.6	250 m upstream from fault trace: 0.3 – 0.8	500 m upstream: 0.06 to 0.40 (mean: 0.22) 250 m upstream: 0.11 to 0.88 (mean: 0.30)
S_{mf}	1.1 – 1.3	1.6 – 2.3	< 1.5	1.8 – 2.3	1.24 (whole mountain front) 1.17 (NW segment) 1.32 (SE segment)
Cross-valley profile	“V”	“U”	“V”	“V”	Soft “V”
Piedmont landforms	Incised alluvial fans	Incised alluvial fans	Short, high-slope, non-incised alluvial fans; channels not connected with the axial fluvial system	Short, gentle-slope alluvial fans, incision only at the apex; channels partially connected with the axial fluvial system	Short, moderate-slope, incised and non-incised alluvial fans; only major streams connected with the axial fluvial system
Mountain front landforms			Well-conserved triangular facets	Degraded or buried mountain front landforms	Well-conserved triangular facets
Slip rate	0.5 mm/year	0.05 mm/year	≥ 0.08 mm/year	0.03-0.07 mm/year	0.07-0.33 mm/year
	Empirically assigned				Calculated from geologic markers

Table 4. Classification of the Concud fault activity, based on quantitative and qualitative features of the fault-generated mountain front and the piedmont. Right column: parameters of the Concud fault used to classify it according to McCalpin [7] and Silva *et al*. [8]